THE JOURNAL OF PHYSICAL CHEMISTRY B

Article

pubs.acs.org/JPCB

Modeling of Polyelectrolyte Adsorption from Micellar Solutions onto Biomimetic Substrates

Soumi Banerjee,[†] Colette Cazeneuve,[‡] Nawel Baghdadli,[‡] Stéphanie Ringeissen,[‡] Fabien Léonforte,*[,‡] Frans A.M. Leermakers,*[,†] and Gustavo S. Luengo*[,‡]

[†]Physical Chemistry and Soft Matter, Wageningen University and Research, Stippeneng 4, 6708 WE Wageningen, The Netherlands

[‡]L'Oréal Research and Innovation, 1 Av. Eugene Scheuller, 93600 Aulnay sous Bois, France

ABSTRACT: Depositing cationic polyelectrolytes (PEs) from micellar solutions that include surfactants (SU) onto surfaces is a rich, complex, highly relevant, and challenging topic that covers a broad field of practical applications (e.g., from industrial to personal care). The role of the molecular architecture of the constituents of the PEs are often overruled, or at least and either, underestimated in regard to the surface properties. In this work, we aim to evaluate the effect of a model biomimetic surface that shares the key characteristics of the extreme surface of hair and its concomitant chemo- and physisorbed properties onto the deposition of a complex PEs:SU system. To tackle out the effect of the molecular architecture of the PEs, we consider (i) a purely linear and hydrophilic PE (P_{100}) and (ii) a PE with lateral amphiphilic chains (PegPE). Using numerical self-consistent field calculations, we show that the architecture of the constituents interfere with the surface properties in a nonintuitive way such that, depending on the amphiphilicity and hydrophilicity of the PEs and the hydrophobicity of the surface, a re-entrant adsorbing transition can be observed, the lipid coverage of the model hair surface being the unique control parameter. Such a behavior is rationalized by the anticooperative associative properties of the coacervate micelles in solution, which is also controlled by the architecture of the PEs and SU. We now expect that PEs adsorption, as a rule, is governed by the molecular details of the species in solution as well as the surface specificities. We emphasize that molecular realistic modeling is essential to rationalize and optimize the adsorption process of, for example, polymer conditioning agents in water-rinsed cosmetic or textile applications.

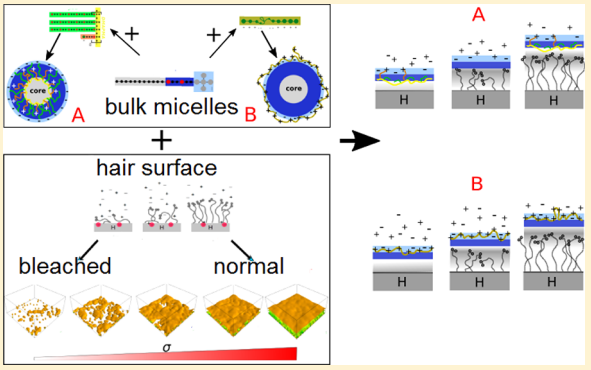

1. INTRODUCTION

Selective adsorption of one component from a mixture of several combined components onto a surface is of huge industrial relevance. In order to tune and control this adsorption process, one often resort to polymer-based smart surfaces (i.e., surfaces with grafted or deposited polymers that can modify the adsorbed states in response to external stimuli). Such responsive surfaces are nowadays widely used in a broad field of versatile applications such as immobilizing biophysical objects like cells or proteins,[1,2] as well as reactive ligands to locally tune friction and adhesion.[3−7] When these surfaces comprise grafted polyelectrolytes (PEs) they also find applications in controlled release for drug delivery[8−11] because they demonstrate significant variations in swelling as a function of pH and ionic strength (IS). Furthermore, the combination of multicomponent responsive polymers grafted on bare surfaces also constitutes versatile strategies to influence, select, and tune the uptake/release of nanoparticles,[12−16] with potential applications in dusty flow regeneration or regenerative medicine[17] as well as for biosensors and actuators.[18−27] Their increasing relevance explains the surge of recent investigations employing a multipronged approach involving chemistry, biology, and engineering that gives also rise to a new field of study named "Biomimetic materials chemistry".[28]

In cosmetics and dermatology, biointerfaces (i.e., membranes) and surfaces (i.e., hair and skin) are a natural example of smart surfaces. Their response and adaptation to the surrounding biological or external environment depend on their biological function and surface chemistry and is in turn extremely complex and very dynamic. In the case of keratin fibers (that are constituents of human hair), the outermost surface is composed of a monolayer of covalently linked fatty acids[29−36] that are exposed to external stimuli such as UV[37] or oxidative treatments.[38] As a response to these, the coverage of the hydrophobic layer can change considerably to the extent that the proteins underneath are exposed and the surface becomes more hydrophilic.[39] In that sense, the hair surface is representative of more complex biological surfaces for whom proteins, sugars, lipids or fatty-acids, among others, react (or degrade) in response to the environmental conditions. Furthermore, the main advantage of the

Received: May 30, 2017
Revised: August 22, 2017
Published: August 23, 2017

DOI: 10.1021/acs.jpcb.7b05195
J. Phys. Chem. B 2017, 121, 8638−8651

hair surface in comparison to other biological ones resides in his stability. It therefore provides a good introduction to the understanding of more complex biomimetic surfaces.

Surface conditioning of hair fibers (i.e., by shampoos), and the extent of textiles (i.e., by washing powders or detergents) that are both influenced by moisture and humidity, is an essential process that facilitates fiber or cloth handling, manageability, and sensoriality. In many cases, PEs are chosen for conditioning due to their adsorption potential onto charged interfaces and their capabilities to reduce the frictional behavior of fibers in a humid environment.[40] In general, the mechanism of action relies on the adsorption upon water rinsing of the complex formed between the polymers and oppositely charged surfactants (SUs) in solution.[41]

In this work, we aim to explore the sceneries responsible of the synergistic effect of the PEs:SU mixture on the adsorption on humanlike hair surface, this, using numerical self-consistent field calculations. We are more specifically focused on modeling the cationic PEs performance in the presence of negatively charged SUs such as sodium lauryl ether sulfate (SLES), a widely used washing agent in cosmetics, and its effect on the adsorption onto hydrophilic hair surface decorated by hydrophobic molecules such as fatty acid chains. This problem is challenging under many aspects, and one among them is that the adsorption takes place from a solution that contains PEs-decorated-SUs micelles. We have shown in a previous work[42] that the structure and stability of such micelles depend on the packing parameter of the SUs[43,44] and critically on the architecture on the segment level of the PEs. The importance of the chain chemistry is of course deeply rooted in the experimental arena but often neglected or only very recently addressed[45−47] by the polymer modeling community which typically focuses on generic features rather than on molecular specificity.

In the following, we integrate this knowledge to the deposit of the PEs:SU complex onto a surface with nontrivial molecular features and concomitant responsiveness, for which more than just quantitative differences show up. The surface is basically considered as hydrophobic, and its complexity and hydrophobicity is tuned by end-tethered fatty acid-like chains whose grafting density σ is the control parameter. Such model substrates qualitatively capture the structure of many natural biosurfaces where lipids are covalently attached to proteins.[48−51] In the case of natural keratin fibers, it is well-known that these lipids are at the origin of their natural hydrophobic character.[36] Still, weathering or chemical treatments for example can disrupt the continuity of this layer, expose proteinaceous groups at the surface, and alter the charge density, in particular, through generating sulfonate groups (i.e., cysteic acid anions) that increase the effective hydrophilic character.[39]

In this paper, we demonstrate that adsorption onto such complex surface is highly molecule specific. The self-consistent field theory of Scheutjens and Fleer[52,53] (SF-SCF) is used to illustrate this. The formalism is well-suited to describe, at the coarse-grained level, SU and PEs molecules of complex architecture without loss of molecular and relevant realistic details. Additionally, the computational efficacy of the numerical scheme allows to account for experimentally relevant short-range solvency effects, including longer-range electrostatics. Combining these advantages, complex problems involving adsorption and self-assembly of PEs:SU complexes become computationally tractable within a time-window below the hour on a local computer. Details about the framework can be found in many previous works.[42,52−57] Key approximations and most of the details that are implemented in the context of the present study are described in Appendix C at the end of this paper. One issue, namely the coupling of the micellar calculations, is a relatively novel aspect which deserves a few comments.

The idea is to study adsorption of SU and PEs molecules on surfaces from a solution that consists of PE-decorated micelles. In the SF-SCF approach, a one-gradient spherical lattice is used to model the complexation of the PE's with surfactant micelles. We reported about this in a previous study,[42] and details are presented below. The outcome of this study is illustrated in Figure 1b. Without going into too much detail, it is necessary to

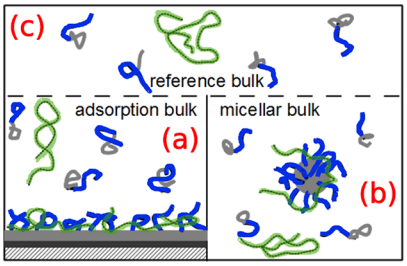

Figure 1. Illustration of the computational strategy. (a) The adsorption system with an adsorption bulk, on top. (b) A most likely micelle surrounded by a micellar bulk. (c) The reference bulk phase which is in equilibrium with both systems (a) and (b) and provides the coupling between these two systems. In this illustration, the concentration ratio of polymer versus surfactant in the bulk phases is not to scale; in the micelle and on the surface, the ratio is more realistic. In reality, the partitioning of long PE chains is extremely shifted toward the complexed phases (mixed micelle/mixed adsorption layer). Ions are not indicated. In (a), substrate is dashed, fatty acids layer is in dark gray, surfactant tails are gray and heads blue, whereas PE is green-dashed. The micellar core in (b) is gray because it is mostly composed of tails of surfactants.

mention that the volume per micelle is linked to the grand-potential of such micelle (hence in reality the complete system consists of many of such micelles) and that the chemical potentials can be computed from the volume fractions of the freely dispersed species surrounding the micelles (micellar bulk). There exist a reference bulk, depicted in Figure 1c that, composition-wise, is the same as the solution surrounding the micelles. In other words, the reference bulk consists of an homogeneous distribution of molecules that have the same chemical potential as the molecules in the micellar solution (but no micelles). In the current calculations, we use a one-gradient planar lattice that allows us to study adsorption phenomena. The typical outcome is sketched in Figure 1a. The interfacial layer is in equilibrium with an "adsorption bulk" solution which again consists of a homogeneous freely dispersed surfactant/PE mixture. This bulk solution is also in equilibrium with the reference bulk of Figure 1c. In other words, the compositions/chemical potentials of the "adsorption bulk" and "reference bulk" phases are identical.

The complication in SCF is that both in the "adsorption bulk" as in the "micellar bulk" the presence of freely dispersed PE-decorated micelles can not explicitly be accounted for. Similarly as in the "reference bulk", the micelles are "filtered out". The role of the reference bulk phase is to "transport" information from the micellar system of Figure 1b to the adsorption problem (a). This is how it is implemented: the first step is to compute from the most likely PE/decorated micelle system the relevant chemical potentials (cf, ref 42). From this,

DOI: 10.1021/acs.jpcb.7b05195
J. Phys. Chem. B 2017, 121, 8638−8651

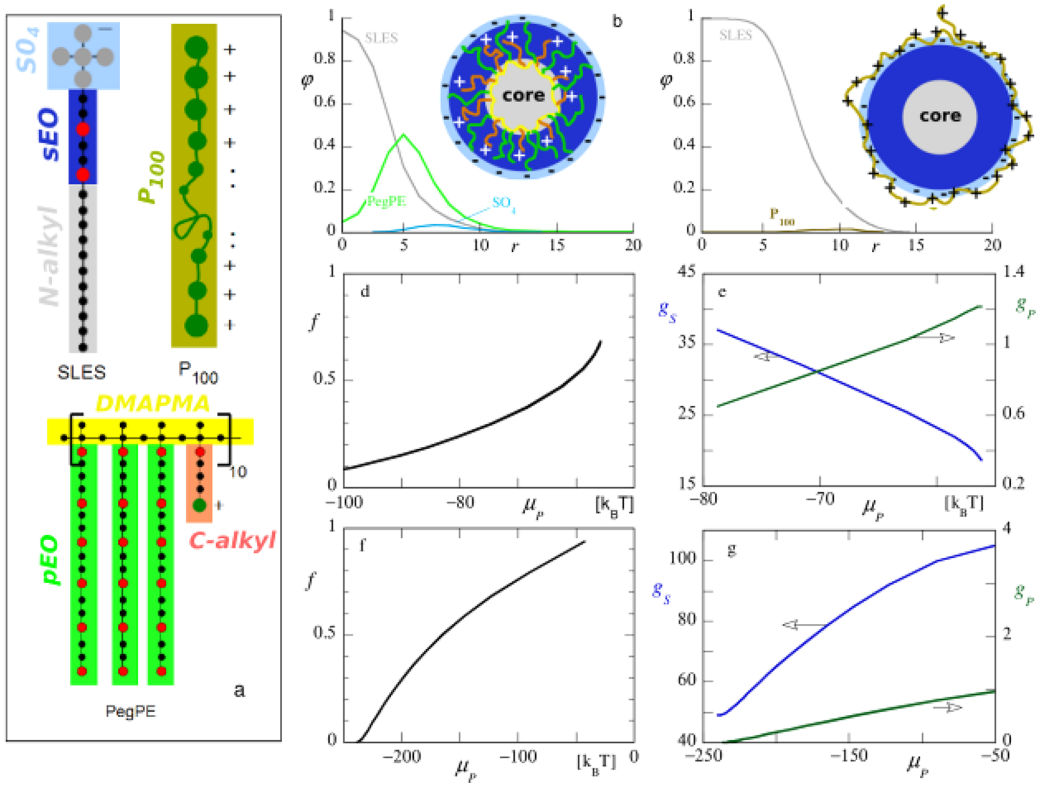

Figure 2. (a) Sketch of SU (SLES) and PEs (P_{100} and PegPE) considered in the simulations. Color coding for the coarse-grained beads: black for hydrophobic CH_3 or CH_2, red for oxygen, gray for sulfate and green for cation. (b and c) Radial volume fraction profiles for SLES:PegPE and SLES:P_{100} mixtures, respectively. Color coding of the micelles follows the one for the blocked-segmental units in (a). (d–e)/(f–g) Charge ratio f in the mixed micelle and aggregation number g for the SLES (g_S) and for the PE (g_p) as a function of the chemical potential, μ_p, of the PE in the bulk, for SLES:PegPE in (d and e) and SLES:P_{100} in (f and g). Salt concentration is fixed to $\varphi^b_{Cl} = 0.001$ (equivalent to $c_s \approx 0.01$ M), and the grand-potential $\Omega(\{\mu\}, V,T)$ of the composite micelles is kept constant to $5k_BT$. See ref 42 for details.

the composition/chemical potentials of the "reference bulk" phase is established. Then in the adsorption problem, the reference bulk phase is taken as an input for the adsorption problem (implying grand-canonical calculations). When this operation is implemented correctly, one will find that there is a strong correlation between the micellar composition and the structure of the interfacial layer. Below, we discuss these correlations. Note that the concentrations suggested in Figure 1 are not to scale. For example, the freely dispersed surfactant concentration is close to the CMC which remains relatively high (because the tail length is not too long; in the illustration, 4 surfactants are in the volume around the micelle). The freely dispersed concentration of the PEs in Figure 1 is, however, strongly exaggerated compared to the freely dispersed surfactants. In reality, this concentration is extremely low, which means that the equilibrium is shifted strongly to the complexed state (most of the PE's are associated with the micelles and very few remain in solution). Similarly, in the adsorption problem most of the PE's are associated with the surfactants at the surface and very few of the PE's are in solution. The chemical potentials in the reference bulk phase communicate this information from the micellar system to the adsorption problem. Typically when the polymer concentrations are very low indeed, the equilibration times become very long. However, in the current problem we have a micellar solution which transports the PE's to the surface, and the equilibration is expected to be fast. Hence, even though the concentration of freely dispersed polymers in the solution is very low, we do expect quick equilibration processes such that an equilibrium SCF analysis is appropriate.

The paper is organized as follows. In section 2, we detail the PEs and SU used in this work and address their interplay in solution. In the next section 3, we provide details and motivations about the description of the biomimetic, model, human hairlike surface. Section 4 compiles the important results on the adsorption of PEs:SU complexes onto the model-hair surface, and we benefit from them to discuss their implication for the interpretation of experimental systems. A brief summary in section 5 concludes the paper.

2. BULK BEHAVIOR

The importance of molecular architecture in relation to surfactant self-assembly is well-known,[43,44] and transporting this problem to PEs:SU mixtures is a natural extent. Recently, using SF-SCF calculations for PEs interacting with oppositely charged micelles, we studied the impact of the molecular structure of the constituents on the nature of the complexes, as well as the bulk phase behavior of these mixtures. We mainly showed that PEs architecture is of key importance for the mode of coassembly with oppositely charged micelles.[42]

In Figure 2a, we detail the molecular structure of the considered PEs. As the subject of the study aims to focus on the role of the chain architecture and charge density, we rationalize our strategy by distinguishing between a purely linear cationic and hydrophilic polymer, P_{100}, and a more sophisticated side-branched cationic and amphiphilic polymer, PegPE. The sketch in Figure 2a shows that P_{100} is modeled as a chain of 100 coarse-grained molecular units (beads) that hold a positive charge. The PegPE polymer, on the other hand, is modeled as a

DOI: 10.1021/acs.jpcb.7b05195
J. Phys. Chem. B 2017, 121, 8638–8651

10 times repeated side-chain motif branched on a hydrophobic backbone, namely a *N*-[3-(dimethylamino)propyl]methacrylamide (DMAPMA) backbone. The side chains are composed of an alternance of 5 ethylene oxide (denoted in Figure 2a as pEO) groups, where in the sketch of the Figure 2a, coarse-grained beads CH_3 or CH_2 and oxygen are colored in black and red, respectively. The PegPE holds a positive charge on a slightly displaced alkyl fragment (C-alkyl) with respect to the other pEO chains.

Both PEs are mixed in solution with a widely used anionic surfactant in cosmetics (i.e., SLES). It is a negatively charged surfactant with a short alkyl tail of 12 C-segments (denoted as *N*-alkyl in Figure 2a) and a few ethylene oxide groups (sEO) that are mimicked, in Figure 2a, by alternating red/black-colored beads. The head groups of SLES are composed of sulfate groups (gray beads) with negative charges. The whole sulfonate head groups (SO_4) at the segmental level are colored in light blue in Figure 2a. The surfactant forms spherical micelles with aggregation numbers of order 50. A more detailed description of the modeled molecular conformations of PEs and SU is provided in Appendix A.

As we aim to extend our previous work[42] to the problematic of deposition on a surface, we summarize in Figure 2 (panels b−g) the main results we obtained under fixed ionic strength 0.01 M. Figure 2 (panels b and c) depict the radial density profiles for each mixture separately, SLES:PegPE in (b) and SLES:P_{100} in (c). We show that for the first system, PE stands with the backbone in the core of the micelle and with charges and EO groups in its corona. Conversely, for the second system, the PE mainly locates in the outer shell (micelle periphery). Such different scenario in the modes of coassembly of the SU:PEs systems should have a drastic impact on the colloidal stability of the mixture. In case (c), we showed that conformations of the PE (loop and tails) that stay in the outer shell of the micelle allow for chain bridges between neighboring micelles, which prevents the colloidal stability. In contrast, for the case (b), the loss of PE chains in the corona of the micelles favors the steric and electrostatic interactions between close micelles, which improves the colloidal stability. To summarize, a hydrophilic cationic PE could destabilize an anionic micellar solution, whereas a much less water-soluble amphiphilic (at the segmental level) cationic PE would stabilize the same micellar solution.

Finally, Figure 2 (panels d−g) depict the binding isotherms for the same systems. In that case, simulations are performed at fixed volume fraction of micelles (i.e., the chemical potential of SLES is the one at which the grand potential $\Omega(\{\mu\},V,T)$ equals $5k_BT$ so that it is above the value at which the first micelle forms), typical for the experimental surfactant formulations. We stress that this specific choice for the grand potential per micelle does not affect our conclusions: a higher value would have implied a somewhat lower micelle concentration and a lower one would have implied a higher micelle concentration; we know that a change in the micelle concentration has little effect on the surfactant chemical potential nor on the micelle size and stability nor on the capacity for PE-binding. We compare in Figure 2 (panels d and e) and (f−g) the dependence in PE chemical potential of the fraction f of SLES charges that is compensated by the PEs and aggregation number g of each components for the SLES:PegPE and SLES:P_{100}, respectively. We note that $f = 1$ means a stocheometric composition of the mixture. In Figure 2d, we observe that for the SLES:PepPE mixture, the PE is mainly bulky and increasing polymer concentration (or its chemical potential μ_p) leads to an increase of the binding that never tends to unity. This means that the complex will depict a non-null zeta potential (typically negatively charged). This will not be the case for the other SLES:P_{100} system, as shown in Figure 2f. For such a PE, increasing the concentration leads to an increase of the loading of polymer on the micelle, and increasing f toward unity or above will strongly destabilize the solution. In the following, we will therefore only consider conditions for which $f < 1$. In Figure 2 (panels e−g), we plot the aggregation number g of SLES (left axes) and PEs (right axes) for PegPE and P_{100}, respectively. We show that when PegPE binds, the number of surfactants per micelle decreases, whereas the other trend emerges for the hydrophilic P_{100} polymer (i.e., its binding leads to an increase of g_S). To summarize, PegPE is locally a weak surfactant and therefore PegPE exchanges with SLES surfactants, whereas in all cases P_{100} complexes with the charged surfactant. In that case, P_{100} screens the repulsion between sulfate head groups of SLES, and more surfactants are needed to increase the osmotic pressure in the corona. Such a compensation mechanism allows one to stabilize the assembly.

It is instructive to rephrase these results[42] in other words. We showed that the interaction of polyelectrolytes with oppositely charged SLES micelles depends strongly on the architecture of the polyelectrolytes. The binding of the model PE:P_{100} on the periphery of the micelles progressively increases the surfactant aggregation number. One may term this cooperative binding. Upon the approach of charge neutralization ($f = 1$), the spherical shape of the surfactant micelles may be compromised and, importantly, also the colloidal stability may be lost. This must be contrasted to the behavior of the PegPE binding on the micelles. As these polymers are on the segment level "amphiphilic", they are positioned at the core−corona interface. The binding is anti-cooperative as an increase in binding the surfactant aggregation number decreases. The complex remains colloidally stable; however, when the complex is driven toward charge neutralization ($f = 1$), the micelle stability is lost due to a depletion of surfactants. Below we will argue that these cooperative or noncooperative modes of binding of the PE's with SLES surfactants is reflected in the mode of binding of these PEs on a fatty acid modified surface.

Importantly, these findings clearly indicate that (1) the electrostatic interactions between the oppositely charged species are important to drive the association at a generic level, but (2) that the chain architectures at the segmental level can dramatically affect conformational features of the complexes. This nontrivial interplay qualitatively leads to different macroscopic behaviors of the solutions.

3. POLYMERS AT INTERFACES

Homopolymers at interfaces is a classical field of research.[58,59] Long polymer chains form self-similar adsorption profiles that can be understood from the knowledge of semidilute polymer solutions. How chemical details can perturb these generic effects is largely unexplored despite the fact that even small segmental features can already shift the expected, generic and ideal behavior to molecular weights that are experimentally inaccessible.[60]

PEs at interfaces represent a much more complex problem because their adsorption onto surfaces becomes a functionof the spatially varying charge density and the salt concentration, c_s. Furthermore, in addition to the usual parameters that dictate the behavior of neutral polymers at interfaces (polymerization degree N, solvent quality through the Flory−Huggins

DOI: 10.1021/acs.jpcb.7b05195
J. Phys. Chem. B 2017, 121, 8638−8651

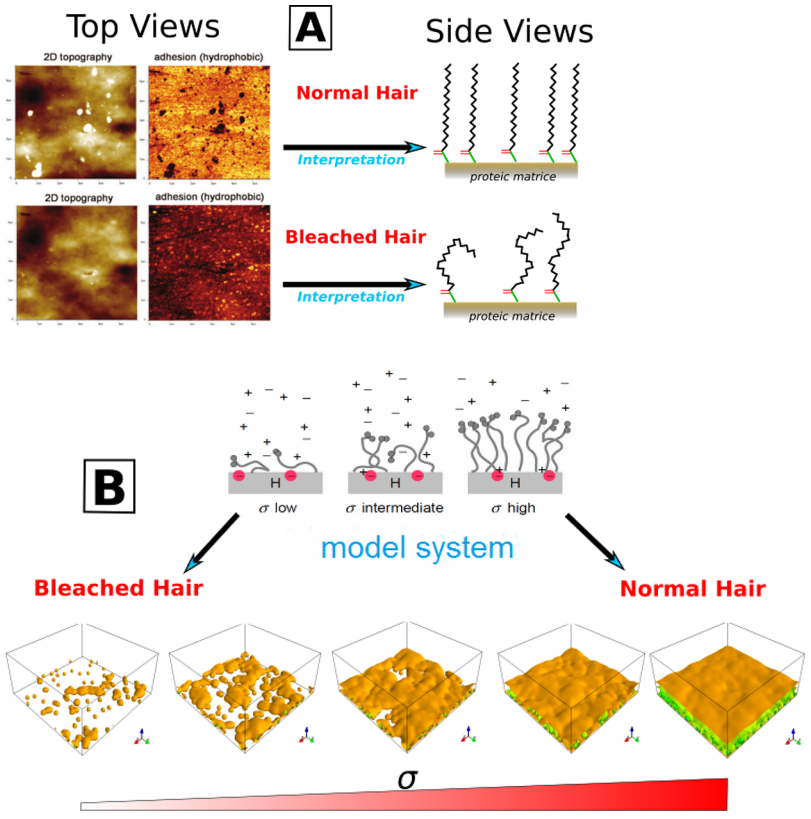

Figure 3. (B) Modeling strategy to mimic the experimental characterization of the normal and bleached hair surface, as depicted in (A). A bare surface, H, is covered by grafted alkyl chains of 20 C-units with a methyl branching at the end (FA). The grafting density, σ, plays the role of the hydrophobic tuning parameter (i.e., high σ corresponds to highly hydrophobic surface and conversely for low σ). The 3D views represent the average, layer-resolved, density profiles of the brush. Topography and adhesion dCFM images for normal (top row) and damaged, bleached, hair surface[39] (bottom row). Dark zones correspond to lower hydrophobic regions and bright to higher. (Right) Corresponding molecular representation based on measurements. Grafted chains are 18-MEA fatty-acids (FA).

parameter χ, polymer density, and surface affinity), PEs will respond differently to the external ionic conditions [i.e., if the degree of charging α on the polymer chain depends on the association−dissociation process of the ionizable groups (weak PEs) or if their degree of charging α is constant in regard to the external conditions (strong PEs)]. It turns out that a new length scale, the Debye length $\kappa_D^{-1} = 0.304/\sqrt{c_s}$ for water, which is representative of the effect of the ionic strength, additionally controls the effect of the screening of the electrostatic interaction. Namely, for low salt concentrations below 0.01 M, the Debye length is large compared to the segmental size of PEs such that charged groups are correlated along the polymer. For a strong PE, this has no effect on the dissociation behavior of these groups, but for a weak PE, whose ionizable groups strongly depends on the local ionic conditions, one has a wide distribution of dissociated and undissociated polymer sites that leads to a shift of the local dissociation constant of the PE-specific dissociation reaction. In that case, changes in the solution pH strongly alter the adsorption[61−63] because the pH interferes with the degree of charging α that, in turn, is non-trivially dependent on the ionic strength and widely distributed among the polymers, leading to strongly heterogeneous electrostatic conditions from the surface. Conversely, for not too low salt concentrations ($c_s \gtrsim 0.1$ M), κ_D^{-1} becomes of the order of the segment size and for weak and strong PEs, charged polymer segments can independently dissociate from each other so that the local electrostatics are effectively screened and the neutral polymer regime is reached. In that regime, adsorption is relatively low because charges give the polymer layer a high effective Flory−Huggins parameter χ (i.e., the second-order virial coefficient that is related to χ and is representative of the excluded volume interactions is strongly repulsive). However, the comparison of theoretical predictions with experiments reveals large deviations,[47,59,64,65] arguably because, in practical situations, molecular specific details as being considered in the present paper seem to play an important role.

As a prerequisite, the study of adsorption of PEs in solution requires deep insights in the bulk behavior. From our bulk study, we know that for a given composite micelle, the polymer and the surfactant have specified chemical potentials and these chemical potentials cannot be chosen independently. They are coupled through the binding isotherms and the thermodynamics of self-assembly. Previously, we considered as most relevant the case where SLES micelles were densely complexed with the PEs; that is, we selected systems close to the end of the binding isotherms (Figure 2, panels d and f). For the problem of adsorption of the mixture, one may need to vary the chemical potentials of the two adsorbing SU and PE species, but it would require one to adapt these changes in concert and consistently with the results from the binding isotherms. Such an approach could become problematic and painful considering the very narrow range of relevant chemical potential of the SU. Therefore, we follow another approach: the tuning parameter for the adsorption is played by the quantity of end-tethered alkyl chains on the bare surface. This approach has two advantages. First, the chains mimic the fatty-acid layer that is relevant

DOI: 10.1021/acs.jpcb.7b05195
J. Phys. Chem. B 2017, 121, 8638−8651

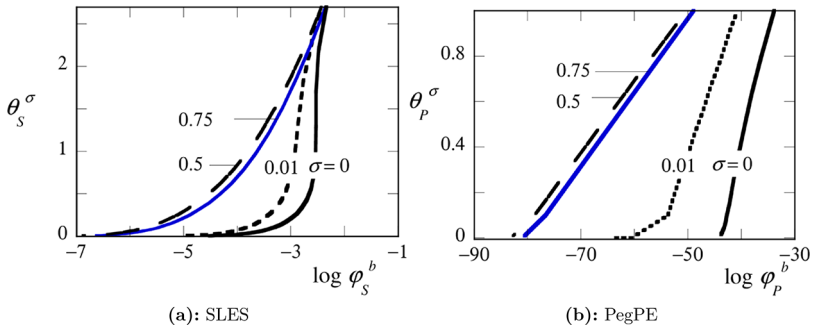

Figure 4. Adsorption isotherms of pure component systems on a hydrophobic surface, H, of varying grafting density σ of FA-alkyl chains as explained in Figure 3. (a) Adsorbed amount, θ_s^σ, of SLES as a function of log φ_S^b, where φ_S^b is the volume fraction in the bulk and (b) of PegPE (θ_P^σ) as a function of log φ_P^b. Volume fraction of salt is φ_s^b = 0.001. The blue-colored curves for the highest grafting density aim to enlighten the nonmonotonic behavior regime.

for hair care applications,[36,48−51] and second, it does not necessitate one to introduce new interaction parameters in the model as fatty acids have chemical structures similar to the tails of SLES.

In Figure 3, we detail the characteristics of the model surface. In addition, it aims to clarify our motivations and strategy for modeling a hairlike interface. The Figure 3A summarizes the top-down approach we aim to follow. On the left part of Figure 3A, and using dynamical chemical force microscopy (dCFM) with CH_3-modified tip in water, it was shown in ref 39 that a significant hydrophobicity decrease appears on bleached hair compared to normal hair, which is in general roughly hydrophobic. Top adhesion maps confirm this decrease in hydrophobicity with the appearance of large quasi-hydrophilic regions for bleached hair. Right part of Figure 3A depicts side views of a proposed interpretation of these experimental results.[39] This interpretation is incorporated in our simulations by a model hairlike surface where the hydrophobic tuning parameter is introduced through the grafting density, σ, of model fatty-acids (FA) chains on a bare surface, H. High σ would provide high hydrophobicity and conversely for low σ. The FA alkyl polymers aim to roughly mimic the chemical architecture of 18-methyleicosanoic acid (18-MEA),[48,50] such that we coarse-grain the chains with grafted C_{20} tails that contain a terminated methyl branch at the free-end.

In biological systems, the surface is basically hydrophobic and bares a net negative charge. However, for sufficiently high σ, the underlying surface properties are of minor importance, and each surface charge acquires a co-ion in its direct vicinity (condensation). In the other limit, we expect that surfactants above their critical micellar concentration (CMC) will form a densely packed layer in the vicinity of H. Therefore, the underneath surface charge will be neutralized by the counterions, and the electrostatic nature of H will not be relevant for the adsorption of the SU:PEs mixture. Hence, in our mean field approach, we neglect the bare surface charge. A forthcoming study will in more detail investigate the effect of the physicochemical properties, surface charge, and electrostatics (pH and ionic strength dependence) on the adsorption of such complexes, based on a combination of previous experimental studies[66] and results from the current modeling strategy. In that spirit, a small step forward is presented in Appendix D, where we incorporate a slight surface charge and compare the adsorption of complexes on the same kind of brush-decorated surfaces. Finally, to ensure that H is inert, we confer its hydrophobic properties so that it is interaction-wise identical to the alkyl grafts. In the following, we fix the bulk volume fraction of salt in our numerical formalism to φ_s^b = 0.001 (which approximately corresponds to $c_s \simeq$ 0.01 M). Details about the other parameters used in the model and the numerical SF-SCF method are provided in the Appendix B and Appendix C, respectively.

Finally, we stress that in the SF-SCF framework, the structure of water is hidden away in the parameter choice, so that in this mean-field approximation, structure of the micelles and adsorbed films do not depend on the water structure. This assumption is roughly correct as long as the study is not intended to address temperature effects, for which fluctuations in the solvent will correlate with chain conformations. In the following, we only use the discretization scheme for water molecules in the SF-SCF theory that aims to primitively mimic the hydrogen-bonding of water with polymers.

To summarize, the current adsorption study includes several "levels" of molecular details: (i) the chemical structure of the SU, (ii) the chemical structure of the PEs, and (iii) the molecular structure of the substrate. In one way or another, these aspects fit together and may largely determine the adsorption features. In the following, we will address the SU:PEs complexes and will respond to the physicochemical nature of the model surface.

4. RESULTS

In Figure 4, we provide results about the individual isotherms onto a bare surface (σ = 0) and increasingly dense fatty-acid grafted surface (σ = 0.01, 0.5, and 0.75). In Figure 4a, we consider the adsorption of SLES from solution up to the critical micellar volume fraction (CMC) of SLES, which is, in the absence of PEs, φ_{SLES} = 0.009 or a chemical potential log $\varphi_{SLES} \approx -2$. The adsorption remains weak up to rather close to the CMC and then increases on a cooperative manner to lead to a monolayer coverage. When FA are grafted on the surface, as depicted in Figure 3, the cooperative effect is less pronounced because one remarks that adsorption already begins at lower volume fraction, φ_{SLES}. Furthermore, we remark that at the CMC, the adsorbed amount is a little bit higher in the case of FA covered surfaces as compared to that on bare H surface. Note that there is a small nonmonotonic dependence as with respect to the role of σ. The adsorption isotherms shift more to the right when the grafting density goes toward its limiting value of unity.

The adsorption isotherm of PegPE, in Figure 4b, depicts well-known features. The scenario involves a mechanism that is in fact strongly related to the nature of the macromolecular

DOI: 10.1021/acs.jpcb.7b05195
J. Phys. Chem. B 2017, 121, 8638−8651

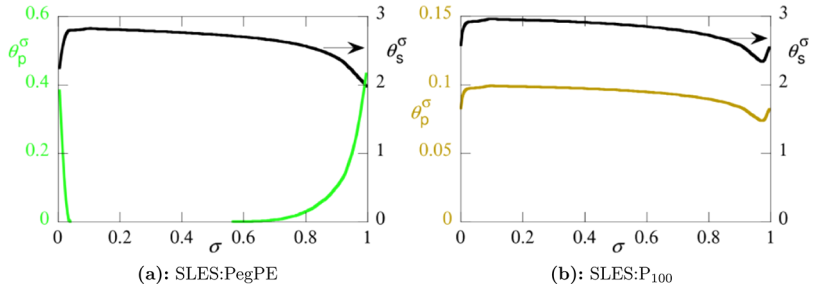

Figure 5. Adsorbed amounts θ^{σ} of SLES (right ordinate) and (a) PegPE, (b) P_{100} (both on left ordinate), as a function of the grafting density, σ, and fixed salt concentration $\varphi^{b}_{Cl} = 0.001$. The fixed chemical potentials are (a) log $\varphi^{b}_{SLES} = -2.4$ and log $\varphi^{b}_{PegPE} = -55.8$ for SLES and PegPE, and (b) log $\varphi^{b}_{SLES} = -3$ and log$\varphi^{b}_{P_{100}} = -52.8$ for SLES and P_{100}.

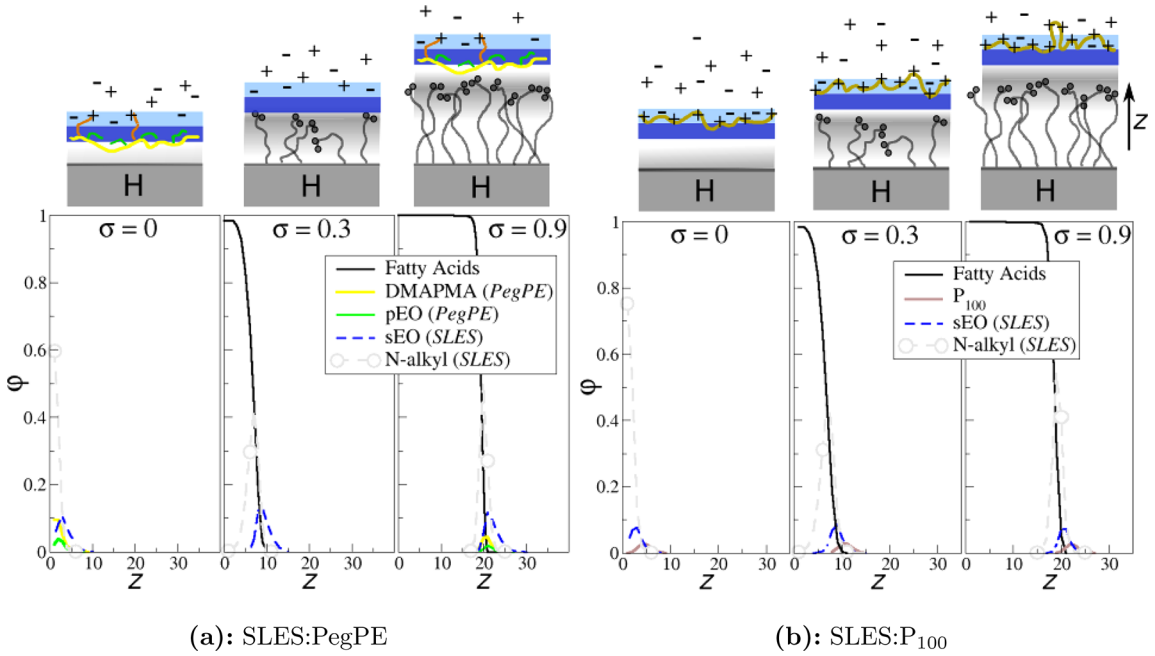

(a): SLES:PegPE (b): SLES:P_{100}

Figure 6. Volume fraction profiles, φ, as a function of the distance z from the surface H for (a) SLES:PegPE and (b) SLES:P_{100}. In all graphs, FA are colored in black, and color coding for the polymers and surfactant blocks are given in Figure 2a and follows the one of Figure 2 (panels b and c). Sketches on the top of each figures (a) and (b) illustrate (using similar colors) the proposed mechanisms of adsorption. The grafting densities of FA chains are σ = 0, 0.3, and 0.9.

structure of the PE. Indeed, one observes chain adsorption, despite the unfavorable electrostatics, already at extremely low concentrations, and that adsorption grows approximately linearly with the chemical potential (logarithm of the volume fraction φ^{b}_{P}) of the polymer in the bulk. Additionally, the plateau adsorption remains modest, namely, below a value of unity meaning below the monolayer coverage. The reason is that, with increasing adsorption, the charge in the layer grows and the electrostatic potential builds up, which prevents new chains to adsorb. In the presence of FA on the surface, the onset of the isotherm occurs at lower volume fractions, but the limiting amount is not strongly affected.

Note again that in the limit of high σ, the isotherms return to the one found for bare, H, surfaces meaning that there is a non-monotonic dependence with respect to the role of σ. We also may mention that purely, hydrophilic, polymer P_{100} hardly adsorbs onto the hydrophobic surface and, consequently, that there is no effect from the grafting density of FA (not shown). One retains from this preliminary study that FA grafting density is, indeed, a reliable and relevant tuning parameter for controlling adsorption of complex SU:PEs mixtures on our model surface.

4.1. Adsorption of PegPE:SLES Complex, a Scenario Case. In the case of the PegPE:SLES mixture, the bulk concentrations favors PegPE micelles with loaded concentrations close to its maximum value. The chemical potentials of the SLES and PegPE are fixed to log $\varphi^{b}_{SLES} = -2.4$ and log $\varphi^{b}_{PegPE} = -55.8$, respectively. We know from the individual isotherms on Figure 4 (panels a and b) that in this case a monolayer of surfactant (SU) forms at the surface, irrespective to the grafting density of the FA chains. Such adsorbed layer of SLES is negatively charged. The positively charged PegPE is expected to locate in a interphase region, and thus to provide an effectively charged surface, because of the electrostatic attraction and the corresponding counterion release mechanism.

In order to elucidate this assumption, we plot in Figure 5a the adsorbed amounts θ^{σ} of both SLES and PegPE as the grafting density, σ, of FA chains increases. The curves are obtained for bulk volume fractions, φ^{b}, of the adsorbing species as specified in the caption of Figure 5. We indeed observe that the adsorbed amount of SLES remains fairly constant throughout the whole range of grafting densities. It only increases at low grafting densities and decreases slightly with

DOI: 10.1021/acs.jpcb.7b05195
J. Phys. Chem. B 2017, 121, 8638−8651

increasing grafting density when $\sigma > 0.6$. The adsorbed amounts are comparable to the amounts found in the adsorption isotherm of Figure 4a. Remarkably, the adsorbed amount of PegPE depicts a strongly pronounced nonmonotonic behavior upon varying σ. Adsorption is observed either at very small or high FA coverage, whereas no adsorption (or at least negligible) occurs within a broad interval of grafting densities. In the $\sigma \approx 0.04$ region, a sharp but continuous adsorption−desorption transition occurs followed by a subsequent smoother and continuous desorption-adsorption transition near $\sigma \approx 0.6$.

This re-entrant adsorption of PegPE cannot be simply attributed to the choice of the interaction parameters defined in Appendix B. Indeed, the surface H as well as the tethered FA chains have all the same type of Flory−Huggins interactions with the solvent, ions, as well as with PegPE. Additionally, changes in the chemical potentials of the components cannot by themselves explain such a re-entrant behavior because all chemical potentials are fixed to the relevant values extracted from our bulk calculations. Furthermore, we noticed in Figure 4a that in the absence of SLES, PegPE do adsorb on the FA layer, but this does not necessarily imply that the SU causes the desorption of PegPE, simply because under the choice of the chemical potentials, PegPE and SLES form composite micelles. We therefore conclude that, apparently, a scenario emerges and from which the fatty acids can perturb the coassembly so that at the specified chemical potentials the same complexes cannot form at the core−corona interface of SLES.

To elaborate on the mechanism, we turn to Figure 6a. One possible scenario is build from the trends of the volume fraction profiles φ, of each SLES, PegPE, and FA species, and for the representative grafting densities of Figure 5a, namely from very low ($\sigma = 0$), intermediate ($\sigma = 0.3$), to very high ($\sigma = 0.9$). For $\sigma = 0$ and $\sigma = 0.9$, the PegPE is able to find location at the core−corona interface of the SLES layer, as it does in Figure 2b for micelle complexes. At intermediate grafting densities $\sigma = 0.3$, PegPE is absent. However, we observe that FA chains interpenetrate the SLES monolayer, and we suspect that these FA chains push the PegPE away. At very low FA density, too few FA chains are available to prevent the incorporation of PegPE, whereas at high grafting density, the monolayer is above the FA layer (or stands above it) so that the FA chains cannot reach the core−corona interface of the SLES monolayer. We know from Figure 2e that the binding of PegPE to SLES micelles reduces the aggregation number of SLES (anticooperative association). Similarly, the adsorbed amount of SLES is highest in the absence of PegPE (at intermediate grafting density) and is relatively low when PegPE has settled inside the SLES monolayer (both at low and high grafting densities). We thus can also argue that in the case when SLES binds very strongly to the FA layer, which occurs at intermediate FA grafting density as suggested in Figure 4a, the packing of SLES surfactants is too high to allow PegPE to go into the SLES monolayer. Only when the adsorbed amount θ_S^σ is close to or below the value found in the isotherm on Figure 4a (bare surface), there is space available for the PegPE chains to intercalate between SLES chains at the core−corona interface. Operationally, this implies that FA chains push the PegPE away, the two species competing for the same position in the layer.

4.2. Adsorption of P_{100}:SLES Complex, a Scenario Case. Similar calculations as done in the previous section 4.1 have been performed for the system wherein SLES surfactant are admixed with P_{100}. For that system, the chemical potentials of each species are fixed to $\log \varphi^b_{SLES} = -3$ and $\log \varphi^b_{P_{100}} = -52.8$ for SLES and P_{100}, respectively. In Figure 5b, we plot the adsorbed amount θ^σ of SLES and P_{100} and, in contrast to the other PegPE:SLES mixture, we do not observe a re-entrant adsorption of the PE. As for the PegPE case, SLES adsorbs on the substrate irrespective of FA grafting densities. However, for all grafting densities the adsorbed amount of P_{100} is proportional to the amount of interfacial surfactants but never drops to zero, unlike for PegPE. We note that the relatively small irregularities at high σ in the curves correspond to the contribution of the methyl branch of the FA, which suppresses the SLES adsorption somehow compared to the naked H surface or the equivalent $\sigma = 1$-like surface.

In Figure 6b, we plot the corresponding volume fraction profiles φ of SLES, P_{100}, and FA. At all σ, we observe a SLES monolayer that is peripherally decorated with the polycationic P_{100}. This suggests the adsorption mechanism in the illustration of Figure 6b. Indeed, as soon as the polycation remains on the outer part of the SLES monolayer, the polycation is always separated from the FA chains. Hence, the FA chains cannot push the cationic polymer away. This effect could have been anticipated from the behavior of the complex in the micellar system. Indeed, as shown in Figure 2g, the micellar association is cooperative, namely the binding of the cationic polymer stimulates SLES-association and the same happens at the FA-covered surfaces. Irrespective of the grafting density, the adsorbed amount of SLES is always higher in the presence of P_{100}, as shown in Figure 5b.

4.3. Discussion. Results from section 4.1 point out that the presence of FA tails, in the vicinity of the region where PegPE may adsorb, is extremely affecting for the PegPE depletion. To test such an impact and its relevance, we introduced in additional numerical investigations, a weak and short-range repulsion between carbons of SLES and those of the grafted alkyl tails. Results are drawn in Appendix D, where we consider that the additional repulsion concerns all FA monomers or only the methyl free-ends of the FA. In the former case, it mainly appears less interdigitation of SLES into the FA layer, and the formation of a negatively charged SLES-populated monolayer located at the top of the FA brush instead of penetrating the brush. Following the arguments developed in section 4.1, the positively charged PegPE develops under such conditions (i.e., undisturbed by the FA layer), a complex with SLES and with an adsorbed amount relatively independent of σ. On the other end, when the methyl free-ends carry the functional, repulsive, interaction, the same kind of re-entrant adsorption as in Figure 6a is observed. Out of the fact that such results confirm the importance of the role of the FA tails, it also provides an additional tuning parameter for controlling adsorption of the complex, namely by customizing the chemical affinity between surfactants and hair's 18-MEA fatty acids.

Understanding the involved mechanisms at interfaces necessitates, as a prerequisite, a detailed knowledge of the bulk behavior of SU:PEs mixtures. In the current study, this is also the case, for many of the results from sections 4.1 and 4.2 could have also been explained from insights gained from the bulk study. However, we mentioned in the preliminary study at the beginning of section 4 that the assembly of PegPE onto SLES micelles was anticooperative. This means that upon binding of PegPE to the SLES micelles, the aggregation number of the SLES micelles decreases. This effect was rationalized from the perspective that PegPE is amphiphilic at the segmental level. From the PegPE perspective, it can be seen as binding occurs onto the SLES layer when this layer is so-to-say shy of SUs.

DOI: 10.1021/acs.jpcb.7b05195
J. Phys. Chem. B 2017, 121, 8638−8651

Alternatively, when the density of SUs is high, only a little amount of PegPE can bind, and when a FA layer covers the surface, the SU also strongly binds to it. Especially at intermediate grafting density. The SU can then insert its tail into this layer and then accumulate at a high density on top of this layer. At such a high SU density, the PegPE cannot bind (i.e., the SU displaces the PegPE layer). In the other limit, in the absence of FA, SU binds to the hydrophobic surface and the SLES layer binds the PegPE similarly, on the same manner as in the bulk, and in an anticooperative way. Similarly, at high grafting density of FA (so that the surface behaves like a barelike surface), the SLES surfactant cannot penetrate into it but has to adsorb onto the FA, dense, layer and again; in that limit, the SLES layer binds the PegPE as in the bulk and in an anticooperative manner. Hence, conceptually, the filtering of PegPE at intermediate grafting density of FA is not only a question of FA-tails disturbance that pushes the PegPE out but rather also results from the strong binding to the SLES, so that FA density is too high to accommodate the PegPE.

5. CONCLUSION

The experimentalist knows that the chain architecture of adsorbing species, as well as the molecular details of the surface on which the adsorption is taking place, are the two most important parameters that determine adsorption. Using self-consistent field simulations and implementing a (coarse-grained) molecularly detailed model for the surfactant (SU), the polyelectrolytes (PEs), and the surface (H + FA), we have studied the scenario where, in the presence of a negatively charged SU, the adsorbed amount of a cationic PE, namely PegPE, can be steered from a non-null value to zero and back, upon an increased grafting density of, FA, alkyl chains grafted on a hydrophobic surface, H. Only for very low and very high grafting densities of the FA chains, the calculated adsorption layer consists of a monolayer of SLES surfactant forming complexes with PegPE. At intermediate grafting density, only the SU monolayer is found on top of the FA-grafts. It is clear that classical adsorption theory cannot cover such intricate adsorption processes. The results exemplify the point that, for polymers at interfaces as well as for polymers that feature in self-assembling processes, the chain architecture is a key parameter. In our previous study, such a concept was confirmed through the formation of PEs-decorated micelles and their impact on the colloidal stability of the coacervat. From the present study, the same appears to be true and deeply relevant for the adsorption process. The theorist's choice of a perfectly flat surface that remains unaltered when the molecules adsorb onto it is not sufficient to explain adsorption processes in complex SU:PEs systems.

From the physico-chemistry point of view, we attributed the numerically predicted re-entrant adsorption of the PegPE (at least in part) to the fact that PegPE is rather bulky and the complex it forms with SLES, to the fact that it is not particularly strong. The cationic PegPE polymer preferably stands at the boundary between the tail-rich core and the water-rich corona. However, the FA grafts can reach this region, and when the perturbation is strong enough, the PegPE preferably forms complexes with the SLES micelles in the bulk rather than with the surface. This mechanism could also explain why an ideal hydrophilic polycation PE like P_{100}, that forms a complex at the periphery of the SLES layer, is invariant with respect to the grafting density of the FA chains, namely, the FA chains cannot reach the outer region of the SU monolayer.

In this paper, we elaborated an example-case and theoretical scenario that aims to point out that molecular architectures can influence the bulk coassembly and surface structures in SU:PEs systems. Undoubtedly many other complex scenario's exist and are deceptively waiting to be unraveled. In the meantime, our observations are important for many industrial processes that use polymer−surfactant mixtures. It is worthwhile to invest more smart polymeric systems that can respond in novel and ingenious ways to external or internal triggers.

APPENDIX A

Architecture of SU and PEs

In our system, we have PEs, SUs, ions, and the remainder is a solvent which we refer to as water. Water consists of starlike clusters occupying 5 sites (this choice is often used to primitively mimic the hydrogen-bonding properties of water). These molecules occupy one-half-space bounded by a planar surface. We do not expect major density variations parallel to the surface, and hence we implement a one-gradient version of the SCF model. Hence, we will specify the z-coordinate which runs normal to the surface. The distribution of the surface component, H, is fixed as a step-profile: $\varphi_H(0) = 1$ and $\varphi_H(z) = 0$ for $z > 0$. The SF-SCF theory implements the SCF equations on a lattice, for which the characteristic size is fixed (here we use $a = 0.3$ nm). The same length is used to split up the molecular components into segments. The segment size equals the lattice size a. We have paid special attention to the architectural properties of the molecules.

The negatively charged SU (SLES) and the positively charged PE (PegPE) are common to our previously published bulk study.[42] SLES is coarse-grained into 23 segments, out of which 5 segments are reserved for the head, sulfate (S_5), groups, whereas the remaining 12 segments for the hydrophobic tail are comprised of carbons (C) and 6 segments that are used to represent the two ethylene oxides (C−C−O). Since SLES headgroup is negatively charged, it is associated with a positive counterion Na^+.

We compare the adsorptive behaviors of two different cationic PEs. The counterions of these PEs are negatively charged species, Cl^-. In the model, the condition is such that the volume fraction in the bulk of the counterion exactly compensates the charge of the PE chain in the bulk.

We consider two different pegylated PE (PegPE) and P_{100} cationic polymers. The first one is composed of a typical backbone with pegylated side chains as well as a side group that carries a positive charge. The two different side groups are present in a 3:1 ratio. Three consecutive side groups consist of an ethylene oxide (PEO) moiety, and the fourth side consists of a charge baring one. Such a quadruplet is repeated 10 times, so each PE chain exactly has 10 positive charges and 30 pending PEO side groups. The charge baring sides have the sequence $O_1C_2X_1$. The PEG sides have a structure $O_1C_1(C_2O_1)5$. As drawn in Figure 2a, the second PE we consider, P_{100}, is a hydrophilic PE composed of 100 hydrophilic segment P. Each segment has a positive charge.

We also have in the system a 1:1 electrolyte couple named Na^+ and Cl^-. These two ions have the same bulk volume fraction. The role of these ions is to independently change the screening of the charges. Both ions are composed of a single united atom. The interaction parameters for Na and Cl ions are all taken similarly, ignoring ion specific effects.

DOI: 10.1021/acs.jpcb.7b05195
J. Phys. Chem. B 2017, 121, 8638−8651

APPENDIX B

Interaction Parameters of SU and PEs

In addition to the molecular description of the species, the model includes short-range interaction parameters (Flory–Huggins parameters χ) between segments of the molecules, dielectric characteristics (ε), and valency (v). The repulsive interactions between the hydrocarbon united atoms and water are the most important ones because this interaction is responsible for the separation of the tails from water phase in such a way that in the core the volume fraction of tails is close to unity, and the same happens for the water volume fraction in the bulk. For instance, a value of $\chi_{Cw} = 1.1$ in Table 1 leads to a critical micellization concentration which decreases roughly by a factor of 10 when the tail length of the surfactant is increased by 3 C units. Such a dependence is well-known in the surfactant literature.[43,44] For all the hydrophilic united atoms implemented in the following, similar type of repulsions with C units are therefore used. With such a choice, we ensure that ions avoid the dense apolar phase. Indeed, in practice, the insertion of ions into a hydrophobic phase is highly energetically unfavorable, and ions may prefer to form ion-pairs in that environment. However, in the SCF method, such an effect is not accounted for, but on the other hand, ions prefer to be dispersed in the high dielectric constant medium like water. In this study, we simply choose to put all the corresponding χ parameters to zero. Also the mutual interaction between hydrophilic units is set to zero.

Table 1. Flory-Huggins Interaction Parameters, χ, between Various Pairs of Segments, Relative Dielectric Constant ε for the Segment Type, and Valency v of the Segment Types as Used in the Simulations[a]

χ	S	O	C	w	Na	Cl	X	H	v	ε
S	0	0	2	0	0	0	0	2	−0.2	80
O	0	0	2	−0.6	0	0	0	2	0	80
C	2	2	0	1.1	2	2	2	0	0	2
w	0	−0.6	1.1	0	0	0	0	2	0	80
Na	0	0	2	0	0	0	0	2	+1	80
Cl	0	0	2	0	0	0	0	2	−1	80
X	0	0	2	0	0	0	0	0	+1	80
H	2	2	0	2	2	2	0	0	0	2
P	0	0	2	0	0	0	0	2	1	80

[a]Here S represents the monomer of the head group (sulfate) in the surfactant, w the monomer in water, C either a CH_3 or CH_2 united atom, and O oxygen in the SU or in the PegPE polymer. Na and Cl are the positive and negative ions from salt, and X denotes the charged group present in the PEs. P corresponds to the monomer in the P_{100} PE and H is the surface.

Finally, we note that a specific negative interaction choice between O and W is taken. This value guarantees the solubility of oxyethylene groups of PegPE or SLES. This choice comes from the unique possibility for water to hydrate a sequence of C_2O_1 units, in regard to the 5 sites description of water in the SF-SCF scheme chosen to mimic water hydrogen-bonding ability. All other parameters are detailed in Table 1.

Hence, we only discuss the ones important for the adsorption calculations. The surface H is hydrophobic, depicts chemical-like affinity $\chi = 2$ or 0 with respect to all hydrophilic units, and $\chi = 0$ with respect to all hydrophobic ones. The same strategy is used for all other segments, namely $\chi = 2$ between hydrophilic and hydrophobic units and 0 between like ones.

The surface is taken hydrophobic with properties identical to the hydrocarbons and one has therefore $\varepsilon = 2$. Also the FA chains do not introduce new Flory–Huggins parameters as these chains only contains the segments of type C equivalent to the tail segments of SLES.

APPENDIX C

SCF Protocol

The SC-SCF method protocol requires the minimization of a mean-field free-energy functional, which is written in terms of volume fraction profiles of all the components, $\varphi_X(z)$, where X is a segment type, and z is the spatial coordinate, and its conjugate segment potential profiles $u_X(z)$. This optimization is done numerically by following the self-consistent field protocol, which states that the volume fractions are a function of the potentials and vice versa. A fixed point of the SCF equations is found by a numerical iterative procedure which delivers results with a precision of at least 7 significant digits, under the constraint that the system is incompressible; that is, that the sum of the volume fractions equal unity for all coordinates z. The method has been elaborated in the literature many times, and thus it suffices to mention just the main approximations.[59]

The single chain partition function of the molecules are the key players in the mean field free energy. We solve these quantities using the Edwards diffusion equation[67] in the dimensionless form:

$$\frac{\partial G(z, s)}{\partial s} = \frac{1}{6}\frac{\partial^2 G(z, s)}{\partial z^2} - u(z, s)G(z, s) \quad (1)$$

which is solved with specified boundary conditions (there is a surface H at $z = 0$, and reflecting boundaries are used at the upper z-coordinate of the system which is far from the surface where bulk conditions prevail and with initial conditions: for the grafted FA chains, we restrict the first segment to be at the surface. All other molecules are allowed to distribute their first segment anywhere in the system. In the SF-SCF approach, the Edwards equation is mapped onto a lattice, which implies a shift of the chain model from a Gaussian chain to the freely jointed chain (FJC). We hasten to mention that this chain model is not exact. It is enforced that two neighboring segments along the chain occupy neighboring coordinates in the lattice. Longer-range correlations along the chain are ignored, which implies that it can occur that a given conformation has more than one segment on a specified lattice site. The incompressibility relation corrects in first order for this excluded-volume problem. A big selling point of the FJC model is that there exists an efficient propagator formalism to obtain the partition function as well as the volume fractions for given segment potentials $u(z, s)$, which is readily generalized for end-grafted chains, as well as for branched chains.

The segment potentials can be computed when the volume fractions are available. Apart from a contribution to enforce the incompressibility of the system, we account for short-range Flory–Huggins-like interaction parameters χ. These parameters are used to compute the interaction energy of a segment at a specified location. The Bragg-Williams mean-field approximation[68] is used to estimate the number of segment–segment contacts. Finally, there are terms in the segment potential that account for the longer-ranged electrostatic potential in the system. These contributionz are similar to the well-known Gouy–Chapman theory, for which we need to solve the Poisson equation

DOI: 10.1021/acs.jpcb.7b05195
J. Phys. Chem. B 2017, 121, 8638–8651

$$\frac{\partial \epsilon(z)}{\partial z}\frac{\partial \psi(z)}{\partial z} = -q(z) \tag{2}$$

where the local dielectric permittivity, ϵ, is chosen to follow a volume fraction weighted average functional. The charge density is given by

$$q(z) = \sum_X \varphi_X(z) e \nu_X \tag{3}$$

where e is the elementary charge and ν_X is the valence (including the sign) of the segment of type X. Note that in our case that the dielectric permittivity is not homogeneous in the system, there is a polarization term in the segment potential, which is not present in the classical Gouy−Chapman theory because in that approach the dielectric permittivity was expected to be constant everywhere in the system.

As previously mentioned, on the lattice surface, H is placed at $z = 0$. And on this surface, we study adsorption. The bulk phase consists of mixed micelles and low amount of free SUs and even lower amounts of free PEs, which is set by the binding isotherms shown in Figure 1 (panels d−g) of the article. After the volume fraction profiles, $\varphi(z)$, are generated, we calculate the excess amount of molecule θ_S^σ and θ_P^σ for the SU and PEs, respectively.

Calculations are typically performed in the grand-canonical ensemble. All volume fractions of the components in the bulk are specified by the input. Again, the exact values are taken from the corresponding bulk calculations that are reviewed in Figure 2. As an outcome, we typically obtain the volume fraction profiles $\varphi_i(z, s)$ for a segment number s at coordinate z. When the sum is taken over all the segments in the molecule, one obtains $\varphi_i(z)$. To quantify the adsorption, we typically focus on the excess adsorption θ_i^σ, which is given in equivalent monolayers by

$$\theta_i^\sigma = \sum_{z=1}^{M} [\varphi_i(z) - \varphi_i^b] \tag{4}$$

where φ^b is the volume fraction in the bulk (which is an input quantity).

APPENDIX D

Effect of FA-Tails/SLES Interaction and Charged Surface H

As mentioned in section 4.3, we aim to evaluate the effect of the nature of the chemical interaction between FA components and SLES on the adsorption of PegPE. For this purpose, we denote systems A, B, and C, the set of interactions where FA and alkyl groups of SLES have the same chemical nature (as in the study presented in the core text fo the article), whereas B corresponds to a system for which only the methyl free-ends of FA depict a weak and repulsive interaction with alkyl branch of SLES, while for C, the whole FA molecule is concerned by such a type of interaction. Numerically, we set $\chi_{\text{M-FA/N-alkyl}} = 0.2$, where M-FA stems from the amount of groups that are concerned by this interaction (i.e., the whole FA chain for C or the free-end for B).

Results for the amount of adsorbed SLES (θ_S^σ) and PegPE θ_P^σ) are plotted in Figure 7a, as a function of the grafting density σ of the FA chains and for the different systems A, B, and C that correspond to the amount of functionalized tails of the FA molecules. We observe that increasing the amount of reactive sites along the FA polymers leads to the disappearance of the re-entrant adsorption of PegPE (system C) and a corresponding decrease of the adsorption of SLES at the top of the brushy surface. When the FA methyl free-ends carry the weak repulsive interaction with alkyl tails of SLES (system B), the re-entrance threshold of PegPE adsorption locates at smaller FA grafting density ($\sigma \sim 0.3$), whereas it is located at $\sigma \sim 0.6$ for the system A.

In Figure 8a, we plot the corresponding volume fraction profiles of the species, in the same spirit as for Figure 6a. For the system C, it mainly appears less interdigitation of SLES into the FA layer compared to systems B and A for which less components of the FA chains carry a repulsive interaction with alkyl groups of SLES. It results that when the whole FA molecules repulses SLES, a negatively charged, SLES-populated, monolayer forms at the top of the FA brush instead of penetrating the brush (for B and A). Hence, the positively charged PegPE can easily bind with SLES without feeling the effect of FA grafting density (which is not the case for systems B and A where SLES can penetrate the brush and FA therefore repel PegPE).

In addition to the effect of the nature of the interaction between the grafted FA and the surfactant, we also addressed the effect of the electrostatic charge of the H surface. Underneath the FA layer, there is a proteineous substrate that acquires a surface charge when the hair is hydrated. The isoelectric point is reported to be on the acidic side. That means that at neutral pH, the surface holds a negative charge. In the following, we get rid of the pH-dependence but rather fix

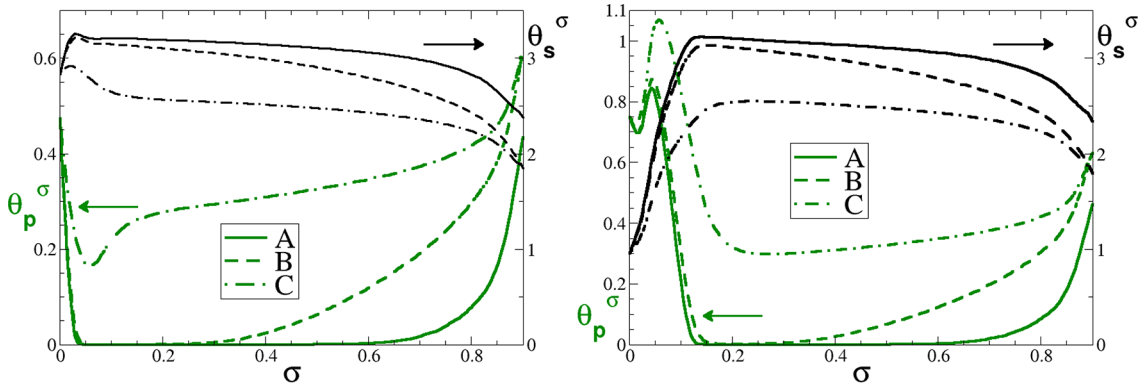

Figure 7. Adsorbed amounts θ^σ of SLES (right ordinate) and PegPE (left ordinate) as a function of the FA grafting density on (a) an uncharged and (b) a slightly negatively charged $\sigma_H = -0.05$ surface H. For each plot, we consider FA chains of the same chemical nature as (A) SLES, with a weak and short-range repulsion between SLES and (B) FA-methyl free-ends and (C) all FA-monomers.

DOI: 10.1021/acs.jpcb.7b05195
J. Phys. Chem. B 2017, 121, 8638−8651

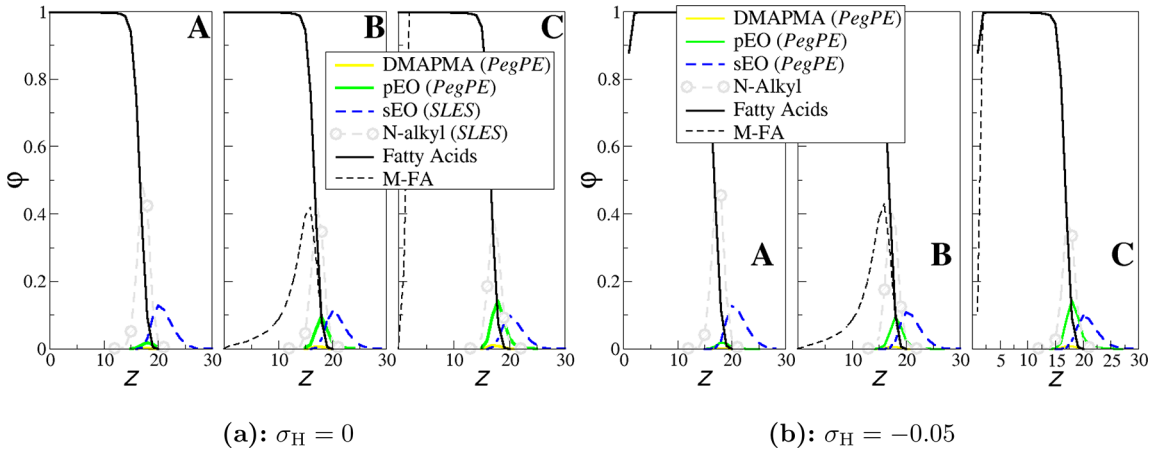

Figure 8. Volume fraction profiles, φ, for (a) uncharged ($\sigma_H = 0$) and (b) charged H surface, and with FA chains of grafting density $\sigma = 0.6$. Same types of FA/SLES interaction as for Figure 7 (panels a and b) are used so that M-FA represents the density of species concerned by the specific FA/SLES interaction.

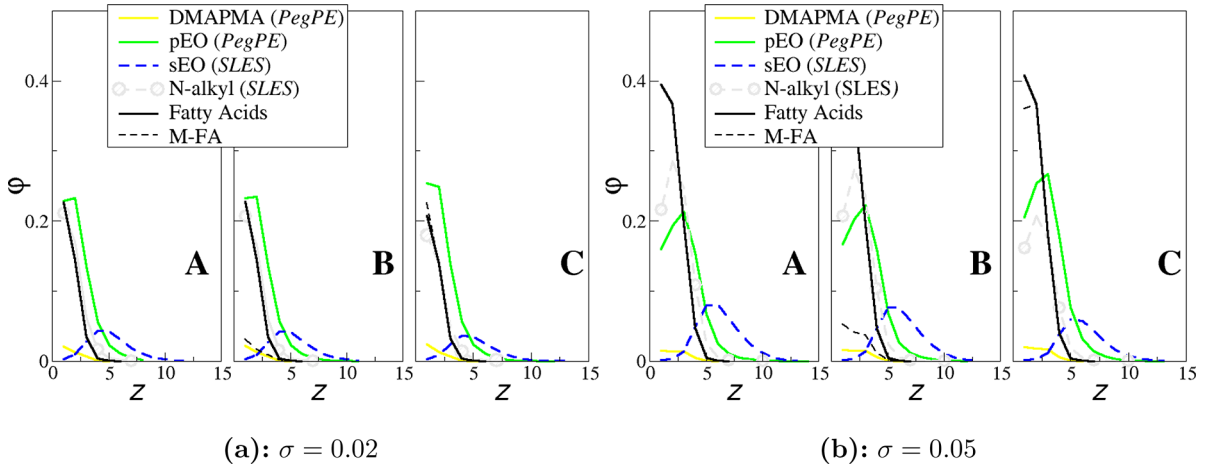

Figure 9. Volume fraction profiles, φ, for a charged surface H ($\sigma_H = -0.05$) and FA chains of grafting density (a) $\sigma = 0.02$ and (b) $\sigma = 0.05$. Same types of FA/SLES interaction as for Figure 7b are used.

the surface charge by setting the dimensionless charge, σ_H per surface site (of area a^2). A value of $\sigma_H = -1$ would imply a surface charge of $-1.6 \times 10^{-19}/(0.3 \times 10^{-9})^2 \simeq -2\text{C/m}^2$, which is an unrealistically high value. More typical values range from $[-10; -100]$ mC/m^2 for low to highly charged substrates, corresponding to $\sigma_H \in [-0.005; -0.05]$.

Because the relative dielectric constant of the FA chains is $2\epsilon_0$, ions may find it unfavorable to penetrate the brush layer, and only at high enough salt concentration (above $\phi_s = 0.001$, i.e., $c_s = 0.05$ M) few counterions will penetrate the brush, leading to a varying electric field profile into the FA layer (nonlinear profile). At high grafting density, however, the surface charge will not be relevant and electrostatics will be screened by the FA chains. But at low FA grafting density, a relatively strong electric field outside the FA layer will modify the effective surface charge that the SU and PegPE will feel.

In Figure 7b, we plot the effect of the surface charge σ_H on the adsorption of SLES and PegPE as the FA grafting density varies and for the different types of interactions A, B, and C of the FA with the alkyl groups of SLES. As anticipated, σ_H strongly modifies the complex adsorption for low FA coverages $\sigma < 0.2$. At very low σ and because of the strong electric field close to the bare surface, negatively charged SLES are deeply impacted and their adsorption strongly decreases whereas cationic PegPE are better adsorbed. Interestingly, slightly increasing FA coverage leads to a better adsorption (close to $\sigma \approx 0.05$), that is even enhanced when all FA monomers carry a weak and repulsive interaction with alkyl groups of SLES (system C).

In order to gather more information about these behaviors, we plot in Figure 9 (panels a and b) the average volume fraction profiles of the different functional blocks of the species, in the low FA coverage region, namely in the dip of adsorption at $\sigma = 0.02$ and the observed peak around $\sigma = 0.05$. In the former case, we observe that alkyl groups of SLES completely fill the layer populated by the FA chains, with a decreasing amount when their mutual interaction becomes repulsive (systems B and C). It turns out that the head (negatively charged) of SLES molecules stays at the top of this layer, which is the less unfavorable region in virtue of the negatively charged surface. On the other hand, PegPE is more attracted by the surface, and polymers fill the accessible space, with a larger amount when *N*-alkyls of SLES are repelled by FA chains (system B and C). A slight increase of the FA grafting density (doubled) is sufficient to screen the electrostatic interaction, unfavorable for SLES, so that more surfactants are adsorbed,

DOI: 10.1021/acs.jpcb.7b05195
J. Phys. Chem. B 2017, 121, 8638−8651

which also favors PegPE adsorption, the formed micelles being still loose enough to allow for PegPE adsorption on the bare surface due to the favorable electrostatic binding. But increasing σ also leads to pushing away the pEO groups of PegPE, and one can anticipate that further increasing FA coverage will favor enthalpic repulsion against electrostatics. In other words, there exists a balance between the gain of being electrostatically adsorbed on the bare surface for PegPE and being repelled by the FA chains because the complex PegPE forms with SLES not strong enough to provide a favorable SU-mediated adsorption.

In the other limit of high FA surface coverage, the surface charge σ_H is expected to not deeply alter the adsorption of the SU:PegPE complex because electrostatics is screened in part. This is confirmed in Figure 7b by the trends of the adsorption curves, but we also observe that amounts of each species adsorbed on the brush is smaller compared to the case where $\sigma_H = 0$. However, average volume fraction profiles, as depicted in Figure 8b, do not show significant differences.

AUTHOR INFORMATION

Corresponding Authors

*E-mail: fleonforte@rd.loreal.com.
*E-mail: frans.leermakers@wur.nl.
*E-mail: gluengo@rd.loreal.com.

ORCID

Fabien Léonforte: 0000-0001-7968-8511
Frans A.M. Leermakers: 0000-0001-5895-2539
Gustavo S. Luengo: 0000-0001-8816-5536

Notes

The authors declare no competing financial interest.

ACKNOWLEDGMENTS

S.B. and F.L. acknowledge support from L'Oréal Research and Innovation, Aulnay-sous-Bois, France.

REFERENCES

(1) Hoy, O.; Zdyrko, B.; Lupitskyy, R.; Sheparovych, R.; Aulich, D.; Wang, J.; Bittrich, E.; Eichhorn, K.-J.; Uhlmann, P.; Hinrichs, K.; et al. Synthetic Hydrophilic Materials with Tunable Strength and a Range of Hydrophobic Interactions. *Adv. Funct. Mater.* **2010**, *20*, 2240−2247.

(2) Advincula, R. C.; Brittain, W.; Caster, K. C.; Rühe, J. *Polymer Brushes Synthesis, Characterization, Application*; Wiley, 2004.

(3) Raviv, U.; Giasson, S.; Kampf, N.; Gohy, J.; Jérôme, R.; Klein, J. Lubrication by Charged Polymers. *Nature* **2003**, *425*, 163−165.

(4) Cao, Q.; Zuo, C.; Li, L.; Zhang, Y. Modulation of Electroosmotic Flow by Electric Field-Responsive Polyelectrolyte Brushes: a Molecular Dynamics Study. *Microfluid. Nanofluid.* **2012**, *12*, 649−655.

(5) Wei, Q.; Cai, M.; Zhou, F.; Liu, W. Dramatically Tuning Friction Using Responsive Polyelectrolyte Brushes. *Macromolecules* **2013**, *46*, 9368−9379.

(6) Drechsler, A.; Synytska, A.; Uhlmann, P.; Elmahdy, M.; Stamm, M.; Kremer, F. Interaction Forces between Microsized Silica Particles and Weak Polyelectrolyte Brushes at Varying pH and Salt Concentration. *Langmuir* **2010**, *26*, 6400−6410.

(7) Drechsler, A.; Synytska, A.; Uhlmann, P.; Stamm, M.; Kremer, F. Tuning the Adhesion of Silica Microparticles to a Poly(2-vinyl pyridine) Brush: an AFM Force Measurement Study. *Langmuir* **2012**, *28*, 15555−15565.

(8) Kost, J.; Langer, R. Responsive Polymeric Delivery Systems. *Adv. Drug Delivery Rev.* **2001**, *46*, 125−148.

(9) Bajpai, A.; Shukla, S.; Bhanu, S.; Kankane, S. Responsive Polymers in Controlled Drug Delivery. *Prog. Polym. Sci.* **2008**, *33*, 1088−1118.

(10) Pillai, O.; Panchagnula, R. Polymers in Drug Delivery. *Curr. Opin. Chem. Biol.* **2001**, *5*, 447−451.

(11) Reineke, T. Stimuli-Responsive Polymers for Biological Detection and Delivery. *ACS Macro Lett.* **2016**, *5*, 14−18.

(12) Christau, S.; Thurandt, S.; Yenice, Z.; von Klitzing, R. Stimuli-Responsive Polyelectrolyte Brushes As a Matrix for the Attachment of Gold Nanoparticles: The Effect of Brush Thickness on Particle Distribution. *Polymers* **2014**, *6*, 1877−1896.

(13) Christau, S.; Möller, T.; Yenice, Z.; Genzer, J.; von Klitzing, R. Brush/Gold Nanoparticle Hybrids: Effect of Grafting Density on the Particle Uptake and Distribution within Weak Polyelectrolyte Brushes. *Langmuir* **2014**, *30*, 13033−13041.

(14) Yenice, Z.; Schön, S.; Bildirir, H.; Genzer, J.; von Klitzing, R. Thermoresponsive PDMAEMA Brushes: Effect of Gold Nanoparticle Deposition. *J. Phys. Chem. B* **2015**, *119*, 10348−10358.

(15) Sinha, S.; Das, S. Under-water Adhesion of Rigid Spheres on Soft, Charged Surfaces. *J. Appl. Phys.* **2015**, *118*, 195306.

(16) Diamanti, S.; Arifuzzaman, S.; Genzer, J.; Vaia, R. Tuning Gold Nanoparticle-Poly(2-hydroxyethyl methacrylate) Brush Interactions: From Reversible Swelling to Capture and Release. *ACS Nano* **2009**, *3*, 807−818.

(17) Krishnamoorthy, M.; Hakobyan, S.; Ramstedt, M.; Gautrot, J. Surface-Initiated Polymer Brushes in the Biomedical Field: Applications in Membrane Science, Biosensing, Cell Culture, Regenerative Medicine and Antibacterial Coatings. *Chem. Rev.* **2014**, *114*, 10976−11026.

(18) Tokareva, I.; Minko, S.; Fendler, J.; Hutter, E. Nanosensors Based on Responsive Polymer Brushes and Gold Nanoparticle Enhanced Transmission Surface Plasmon Resonance Spectroscopy. *J. Am. Chem. Soc.* **2004**, *126*, 15950−15951.

(19) Gupta, S.; Agrawal, M.; Uhlmann, P.; Simon, F.; Oertel, U.; Stamm, M. Gold Nanoparticles Immobilized on Stimuli Responsive Polymer Brushes as Nanosensors. *Macromolecules* **2008**, *41*, 8152−8158.

(20) Gupta, S.; Uhlmann, P.; Agrawal, M.; Chapuis, S.; Oertel, U.; Stamm, M. Immobilization of Silver Nanoparticles on Responsive Polymer Brushes. *Macromolecules* **2008**, *41*, 2874−2879.

(21) Wang, T.; Wang, S.; Zhang, X.; Song, G.; Yu, Y.; Chen, X.; Fu, Y.; Zhang, J.; Yang, B. Responsive Etalon Based on PNIPAM@SiO2 Composite Spacer with Rapid Response Rate and Excellent Repeatability for Sensing Application. *Nanotechnology* **2015**, *26*, 285501.

(22) Ferhan, A.; Guo, L.; Zhou, X.; Chen, P.; Hong, S.; Kim, D.-H. Solid-Phase Colorimetric Sensor Based on Gold Nanoparticle-Loaded Polymer Brushes: Lead Detection as a Case Study. *Anal. Chem.* **2013**, *85*, 4094−4099.

(23) Welch, M.; Rastogi, A.; Ober, C. Polymer Brushes for Electrochemical Biosensors. *Soft Matter* **2011**, *7*, 297−302.

(24) Chen, Y.; Gai, P.; Xue, J.; Zhang, J.-R.; Zhu, J.-J. An"ON-OFF" Switchable Power Output of Enzymatic Biofuel Cell Controlled by Thermal-Sensitive Polymer. *Biosens. Bioelectron.* **2015**, *74*, 142−149.

(25) Ashaduzzaman, M.; Anto Antony, A.; Arul Murugan, N.; Deshpande, S.; Turner, A.; Tiwari, A. Studies on an On/Off-switchable Immunosensor for Troponin T. *Biosens. Bioelectron.* **2015**, *73*, 100−107.

(26) Welch, M.; Doublet, T.; Bernard, C.; Malliaras, G.; Ober, C. A Glucose Sensor Via Stable Immobilization of the GOx Enzyme on an Organic Transistor Using a Polymer Brush. *J. Polym. Sci., Part A: Polym. Chem.* **2015**, *53*, 372−377.

(27) Mitsuishi, M.; Koishikawa, Y.; Tanaka, H.; Sato, E.; Mikayama, T.; Matsui, J.; Miyashita, T. Nanoscale Actuation of Thermoreversible Polymer Brushes Coupled with Localized Surface Plasmon Resonance of Gold Nanoparticles. *Langmuir* **2007**, *23*, 7472−7474.

(28) Dujardin, E.; Mann, S. Bio-inspired Materials Chemistry. *Adv. Mater.* **2002**, *14*, 775−788.

(29) Swift, J. Human Hair Cuticle: Biologically Conspired to the Owner's Advantage. *J. Cosmet. Sci.* **1999**, *50*, 23−47.

(30) Bhushan, B. Nanoscale Characterization of Human Hair and Hair Conditioners. *Prog. Mater. Sci.* **2008**, *53*, 585−710.

DOI: 10.1021/acs.jpcb.7b05195
J. Phys. Chem. B 2017, 121, 8638−8651

(31) Negri, A.; Cornell, H.; Rivett, D. A Model for the Surface of Keratin Fibers. *Text. Res. J.* **1993**, *63*, 109−115.
(32) Negri, A.; Rankin, D.; Nelson, W.; Rivett, D. A Transmission Electron Microscope Study of Covalently Bound Fatty Acids in the Cell Membranes of Wool Fibers. *Text. Res. J.* **1996**, *66*, 491−495.
(33) Jones, L.; Rivett, D. The role of 18-Methyleicosanoic Acid in the Structure and Formation of Mammalian Hair Fibres. *Micron* **1997**, *28*, 469−485.
(34) Zahn, H.; Messinger, H.; Hocker, H. Covalently Linked Fatty Acids at the Surface of Wool: Part of the "Cuticle Cell Envelope. *Text. Res. J.* **1994**, *64*, 554−555.
(35) Peet, D.; Wettenhall, R.; Rivett, D. The Chemistry of the Cuticle Surface of Keratin Fibers. *Text. Res. J.* **1995**, *65*, 58−59.
(36) Breakspear, S.; Smith, J.; Luengo, G. Effect of the Covalently Linked Fatty Acid 18-MEA in the Nanotribology of Hair's Outermost Surface. *J. Struct. Biol.* **2005**, *149*, 235−242.
(37) Richena, M.; Rezende, C. Effect of Photodamage on the Outermost Cuticle Layer of Human Hair. *J. Photochem. Photobiol., B* **2015**, *153*, 296−304.
(38) Antunes, E.; Cruz, C.; Azoia, N.; Cavaco-Paulo, A. The Effects of Solvent Composition on the Affinity of a Peptide Towards Hair Keratin: Experimental and Molecular Dynamics Data. *RSC Adv.* **2015**, *5*, 12365−12371.
(39) Korte, M.; Akari, S.; Kühn, H.; Baghdadli; Möhwald, N. H.; Luengo, G. S. Distribution and Localization of Hydrophobic and Ionic Chemical Groups at the Surface of Bleached Human Hair Fibers. *Langmuir* **2014**, *30*, 12124−12129.
(40) Luengo, G.; Galiano, A. In *Aqueous Lubrication*; Spencer, N., Ed.; World Scientific, 2015; Chapter 1, pp 103−144.
(41) Hössel, P.; Dieing, R.; Nörenberg, R.; Pfau, A.; Sander, R. Conditioning Polymers in Today's Shampoo Formulations - Efficay, Mechanism and Test Methods. *Int. J. Cosmet. Sci.* **2000**, *22*, 1−10.
(42) Banerjee, S.; Cazeneuve, C.; Baghdadli, N.; Ringeissen, S.; Leermakers, F. A. M.; Luengo, G. S. Surfactant-polymer interactions: molecular architecture does matter. *Soft Matter* **2015**, *11*, 2504−2511.
(43) Israelachvili, J.; Mitchell, D.; Ninham, B. Dispersion Interaction of Crossed Mica Cylinders -Reanalysis of Israelachvili-Taber Experiments. *J. Chem. Soc. Faraday Trans. 2* **1976**, *72*, 2526−2536.
(44) Israelachvili, J.; Marcelja, S.; Horn, R. Physical Principles of Membrane Organization. *Q. Rev. Biophys.* **1980**, *13*, 121−200.
(45) Angelescu, D.; Linse, P. Branched and Linear Polyion Complexes at Variable Charge Densities. *J. Phys.: Condens. Matter* **2015**, *27*, 355101.
(46) Angelescu, D.; Linse, P. Branched & Linear Polyion Complexes Investigated by Monte Carlo Simulations. *Soft Matter* **2014**, *10*, 6047.
(47) Xie, F.; Turesson, M.; Woodward, C.; van Gruijthuijsen, K.; Stradner, A.; Forsman. Theoretical Predictions of Structures in Dispersions Containing Charged Colloidal Particles and Non-adsorbing Polymers. *Phys. Chem. Chem. Phys.* **2016**, *18*, 11422−11434.
(48) McMullen, R.; Kelty, S. Molecular Dynamic Simulations of Eicosanoic Acid and 18-Methyleicosaneic Acid Langmuir Monolayers. *J. Phys. Chem. B* **2007**, *111*, 10849−10852.
(49) Natarajan, U.; Robbins, C. The Thickness of 18-MEA on an Ultra-high-sulfur Protein Surface by Molecular Modeling. *J. Cosmet. Sci.* **2010**, *61*, 467−478.
(50) Cheong, D.; Lim, F.; Zhang, L. Insights into the Structure of Covalently Bound Fatty Acid Monolayers on a Simplified Model of the Hair Epicuticle from Molecular Dynamics Simulations. *Langmuir* **2012**, *28*, 13008−13017.
(51) Habartova, A.; Roeselova, M.; Cwiklik, L. Investigation of Mixed Surfactant Films at Water Surface using Molecular Dynamics Simulations. *Langmuir* **2015**, *31*, 11508−11515.
(52) Scheutjens, J. M. H. M.; Fleer, G. J. Statistical Theory of the Adsorption of Interacting Chain Molecules. 1. Partition Function, Segment Density Distribution, and Adsorption Isotherms. *J. Phys. Chem.* **1979**, *83*, 1619−1635.
(53) Scheutjens, J. M. H. M.; Fleer, G. J. Statistical Theory of the Adsorption of Interacting Chain Molecules. 2. Train, Loop, and Tail Size Distribution. *J. Phys. Chem.* **1980**, *84*, 178−190.
(54) Evers, O. A.; Scheutjens, J. M. H. M.; Fleer, G. J. Statistical Thermodynamics of Block Copolymer Adsorption. 1. Formulation of the Model and Results for the Adsorbed Layer Structure. *Macromolecules* **1990**, *23*, 5221−5233.
(55) Evers, O. A.; Scheutjens, J. M. H. M.; Fleer, G. J. Statistical Thermodynamics of Block Copolymer Adsorption. Part 2.-Effect of Chain Composition on the Adsorbed Amount and Layer Thickness. *J. Chem. Soc., Faraday Trans.* **1990**, *86*, 1333−1340.
(56) Leermakers, F.; Scheutjens, J. Statistical Thermodynamics of Associated Colloids. V. Critical Micelle Concentration, Micellar Size and Shape. *J. Colloid Interface Sci.* **1990**, *136*, 231−241.
(57) Jódar-Reyes, A.; Leermakers, F. Self-Consistent Field Modeling of Linear Nonionic Micelles. *J. Phys. Chem. B* **2006**, *110*, 6300−6311.
(58) De Gennes, P. *Scaling Concepts in Polymer Physics*; Cornell University Press: Ithaca, NY, 1979.
(59) Fleer, G.; Cohen Stuart, M.; Scheutjens, J.; Cosgrove, T.; Vincent, B. *Polymers at Interfaces*; Chapman and Hall: London, 1993.
(60) Charlaganov, M.; Kosovan, P.; Leermakers, F. New Ends to the Tale of Tails: Adsorption of Comb Polymers and the Effect on Colloid Stability. *Soft Matter* **2009**, *5*, 1448−1459.
(61) Blaakmeer, J.; Bohmer, M.; Cohen-Stuart, M. A.; Fleer, G. Adsorption of Weak Polyelectrolytes on Highly Charged Surfaces, Poly (acrylic acid) on Polystyrene Latex with Strong Cationic Groups. *Macromolecules* **1990**, *23*, 2301−2309.
(62) Vagharchakian, L.; Desbat, B.; Hénon, S. Phase Diagram for the Adsorption of Weak Polyelectrolytes at a Soft Charged Surface. *J. Phys. Chem. B* **2006**, *110*, 22197−22201.
(63) Flood, C.; Cosgrove, T.; Espidel, Y.; Howell, I.; Revell, P. Sodium Polyacrylate Adsorption onto Anionic and Cationic Silica in the Presence of Salts. *Langmuir* **2007**, *23*, 6191−6197.
(64) Cohen Stuart, M.; Fleer, G. J.; Lyklema, J.; Norde, W.; Scheutjens, J. Adsorption of Ions, Polyelectrolytes and Proteins. *Adv. Colloid Interface Sci.* **1991**, *34*, 477−535.
(65) Dias, R.; Pais, A.; Linse, P.; Miguel, M.; Lindman, B. Polyion Adsorption onto Catanionic Surfaces. A Monte Carlo Study. *J. Phys. Chem. B* **2005**, *109*, 11781−11788.
(66) Guzman, E.; Ortega, F.; Baghdadli, N.; Cazeneuve, C.; Luengo, G.; Rubio, R. Adsorption of Conditioning Polymers on Solid Substrates with Different Charge Density. *ACS Appl. Mater. Interfaces* **2011**, *3*, 3181−3188.
(67) Edwards, S. The Statistical Mechanics of Polymers with Excluded Volume. *Proc. Phys. Soc., London* **1965**, *85*, 613−624.
(68) Hill, T. *An Introduction in Statistical Thermodynamics*; Addison-Wesley Pubisher: London, 1960.

DOI: 10.1021/acs.jpcb.7b05195
J. Phys. Chem. B 2017, 121, 8638−8651